

TOWARD UNDERSTANDING THE ORIGIN OF TURBULENCE IN MOLECULAR CLOUDS:
— SMALL SCALE STRUCTURES AS UNITS OF DYNAMICAL MULTI-PHASE INTERSTELLAR MEDIUM—

KENGO TACHIHARA^{1, 2}, KAZUYA SAIGO², AYA E. HIGUCHI^{1, 2}, TSUYOHSHI INOUE³, SHU-ICHIRO INUTSUKA⁴, MORITZ HACKSTEIN⁵, MARTIN HAAS⁵, MARKUS MUGRAUER⁶

(Accepted May 19, 2012)
Draft version November 2, 2018

ABSTRACT

In order to investigate the origin of the interstellar turbulence, detailed observations in the CO $J = 1-0$ and $3-2$ lines have been carried out in an interacting region of a molecular cloud with an H II region. As a result, several 1,000 to 10,000 AU scale cloudlets with small velocity dispersion are detected, whose systemic velocities have a relatively large scatter of a few km s^{-1} . It is suggested that the cloud is composed of small-scale dense and cold structures and their overlapping effect makes it appear to be a turbulent entity as a whole. This picture strongly supports the two-phase model of turbulent medium driven by thermal instability proposed previously. On the surface of the present cloud, the turbulence is likely to be driven by thermal instability following ionization shock compression and UV irradiation. Those small scale structures with line width of $\sim 0.6 \text{ km s}^{-1}$ have a relatively high CO line ratio of $J = 3-2$ to $1-0$, $1 \lesssim R_{3-2/1-0} \lesssim 2$. The large velocity gradient analysis implies that the 0.6 km s^{-1} width component cloudlets have an average density of 10^{3-4} cm^{-3} , which is relatively high at cloud edges, but their masses are only $\lesssim 0.05 M_{\odot}$.

Subject headings: Turbulence – ISM: structure – ISM: clouds – ISM: kinematics and dynamics – stars: formation

1. INTRODUCTION

Understanding the physical mechanism of contraction and condensation of molecular cloud cores toward star formation is a long standing issue. To date, two major paradigms have been proposed. First is that cores are in a magnetically subcritical state, and as the magnetic field dissipates by ambipolar diffusion they collapse quasi-statically (magnetic model; Shu et al. 1987). The other model is that the interstellar medium (ISM) is dominated by supersonic turbulence and the collision of the turbulent flow forms temporary density enhancements, some of which undergo gravitational collapse (turbulent model; Mac Low & Klessen 2004). The magnetic model is favored by some theoretical studies because the magnetic field can be modeled to have arbitrary strength and configurations (aligned or disordered). It is, however, very difficult to be investigated observationally, being a 3-dimensional vector field. On the other hand, turbulence is ubiquitous in interstellar space. Almost all molecular line emission observed in molecular clouds have larger line widths than those expected from their thermal sound speed. A difficulty of the turbulent model is its unknown nature, namely the origin of the turbulence. The interstellar turbulence must have a much shorter dissipation

timescale than lifetime of dense cores because its supersonic flow forms shocked regions and the energy is rapidly lost by radiation. The turbulent model requires a driving mechanism to keep itself over a long timescale.

These two models are supported by some observational evidence. Low density diffuse clouds in general have filamentary structures, where aligned magnetic field lines (parallel or perpendicular to the long axis) are often observed (e.g., Myers & Goodman 1991). These indicate that the ISM is frozen onto the magnetic field lines rather than bound by self-gravity. Molecular cloud cores are, on the other hand, reported to be dominated by turbulence, and those forming stars tend to have relatively small line widths (Tachihara et al. 2002). This suggests that as interstellar turbulence dissipates, cores tend to get gravitationally bound, condensed, and form stars. It is also shown that the amount of turbulence is different among regions possibly due to difference in the environment; for example, cores in Taurus have much smaller line widths than those in Ophiuchus North and Lupus where star formation is not active and the timescale of core evolution is supposed to be longer (e.g., Tachihara et al. 2000a, 2002). Hence, turbulence is suggested to be one of the key elements controlling star formation activity. For these reasons, investigating the origin and driving mechanism of turbulence is vitally important for determining the timescale and necessary conditions of star formation. A clue may be in the environment, namely, many OB stars are distributed in the Ophiuchus North and Lupus regions where cores have relatively large line width. A strong UV radiation field is known to affect kinematics and morphology of molecular clouds (e.g., Lefloch & Lazareff 1994).

A promising theoretical model for the origin of interstellar turbulence was proposed by Koyama & Inutsuka (2000, 2002) and following studies (Yamada et al.

k.tachihara@nao.ac.jp

¹ Joint ALMA Observatory, Alonso de Córdova 3107, Vitacura, Santiago, Chile

² National Astronomical Observatory of Japan, 2-21-1, Osawa, Miaka, Tokyo, 181-8588, Japan

³ Department of Physics and Mathematics, Aoyama Gakuin University, Fuchinobe, Sagami-hara 229-8558, Japan

⁴ Department of Astrophysics, Nagoya University, Chikusa-ku, Nagoya, 464-8602, Japan

⁵ Astronomisches Institut, Ruhr-Universität Bochum, Universitätsstr. 150, D-44801, Bochum, Germany

⁶ Astrophysikalisches Institut und Universitäts-Sternwarte Jena, Schillergäßchen 2-3, D-07745, Jena, Germany

2007; Inoue & Inutsuka 2008, 2009a; Hennebelle & Audit 2007; Hennebelle et al. 2007). Their model (hereafter the two-phase medium model) suggests that shock compressed layers of the interstellar diffuse gas undergo thermal instability and fragment into small scale (≤ 1000 AU) structures composed of denser cold neutral medium (CNM). They are supposed to coalesce to form larger structures (~ 10000 AU). These cloudlets are embedded in warm neutral medium (WNM), and have random motions (see Fig. 1 of Koyama & Inutsuka 2002). The velocity is supersonic with respect to the sound speed of the CNM ($T \sim 50$ K), but subsonic with respect to that of WNM ($T \sim 8000$ K) (Field et al. 1969; Koyama & Inutsuka 2000). Because of the two-phase medium, turbulence is sustained for relatively long timescales.

In order to corroborate the idea of the two-phase medium model, we intend to detect small scale structures of the molecular cloud and investigate how interstellar turbulence is driven from the clouds' morphological and kinematical structures and their physical properties. We make detailed observations of CO $J=1-0$ and $3-2$ at the surface of the molecular cloud LDN 204 facing an H II region where ionization shock compression is expected to be taking place.

2. TARGET REGION LDN 204

LDN 204 is a filamentary cloud complex facing the Sh 2-27 H II region ($r \sim 5$ pc), that is excited by the nearest O star, ζ Oph (SpT = O9.5V, $d = 140$ pc). This cloud complex was entirely surveyed by the NANTEN telescope in ^{12}CO (HPBW = $2'.7$), and it was found that the cloud is accelerated by illuminating UV radiation (Tachihara et al. 2000b; Liszt et al. 2009). The cloud complex harbours embedded dense cores discovered in C^{18}O , while star formation is not active and no associated young stars have been found (Tachihara et al. 2000a).

The line width of C^{18}O $J=1-0$ observed by the NANTEN telescope in this region is typically as large as ~ 0.74 km s $^{-1}$, significantly larger than that in Taurus (0.49 km s $^{-1}$ in average; Onishi et al. 1996). The strong UV radiation is suggested to have compressed the molecular cloud leading it to form dense cores, while the streaming motions of the low density gas imply considerable kinetic energy input to the ISM (Tachihara et al. 2000b). Noteworthy is that ζ Oph is a run-away star traveling through the region ejected from the center of the Upper Sco subgroup of the Sco OB association. Therefore the entire cloud complex is under the influence of the UV radiation from ζ Oph within a few $\times 10^5$ years.

Another interesting aspect is that the filamentary cloud is penetrated by magnetic field lines perpendicular to the long axis of the filament (McCutcheon et al. 1986). The cloud complex is suggested to be controlled by magnetic fields, while no further investigation toward the dense region has been reported.

Because of the conditions mentioned above, in particular its proximity and the strong UV radiation, we chose the interface region of LDN 204 and Sh 2-27 as the best target for the present study.

3. OBSERVATIONS

3.1. 45 m telescope observations

We carried out CO $J=1-0$ observations at 115 GHz with the NRO 45 m telescope (HPBW = $15''$, corresponding to 2000 AU). The interface region of the cloud surface of $11' \times 22'$ area centered at (R.A., Dec.) $_{J2000} = (16:46:45.0, -12:21:30.0)$ is surveyed with the BEARS multi-beam receiver employing the On-The-Fly (OTF) mapping mode. We repeated the vertical and horizontal scanning many times and summed the data afterward in order to avoid scanning effects. We also employed scaling for correcting the beam efficiency by multiplying the beam-specific factors provided by the Nobeyama observatory. The telescope pointing was checked every 2 hours by obtaining 5-point observations toward nearby SiO maser sources.

Throughout the observing runs, the wind speed has been below 15 m s $^{-1}$. About one fifth of the observations were taken under slightly windy conditions as wind speed was ≥ 10 m s $^{-1}$. We thus divide the data into two to see how the spatial resolution gets worse under the windy conditions. No significant difference between windy and calm conditions can be seen, and eliminating the data with windy conditions worsens the S/N ratio of the final image. We therefore decided to use all the data.

The data taken with the OTF mapping is reduced on the NRO data reduction software called "NOSTAR" (Sawada et al. 2008). The baseline is subtracted by fitting to a linear function. The data is re-gridded into a $7''.5$ grid spacing by convolving with the first order Bessel function \times the Gaussian function, resulting in the final data cube with an effective spatial resolution of $19''.5$. For each spectrum of the $7''.5$ grid cell, a final signal sensitivity of $T_{\text{rms}} = 0.37$ K with a velocity resolution of 0.1 km s $^{-1}$ is achieved.

3.2. ASTE observations

Toward three selected regions where peculiar small scale structures are detected, we made follow-up CO $J=3-2$ observations with the Atacama Submillimeter Telescope Experiment (ASTE). It has a heterodyne receiver working at 345 GHz with typical noise temperature of $T_{\text{sys}} \sim 400$ K (double-sideband) at the zenith. It is equipped with the 1024-channel digital backend that has a frequency resolution of 125 kHz, which corresponds to the velocity resolution of 0.11 km s $^{-1}$. Its 10 m dish enables us to have comparable spatial resolution to the 45 m telescope with the HPBW of $22''$. The two target regions are centered at $(16:46:45.0, -12:22:50)$ and $(16:46:36.5, -12:28:30)$ with sizes of $4' \times 4'$ and $3' \times 3'$, respectively, and are mapped with the OTF mode. The pointing error was corrected every 2 hours measuring the offset from a strong point-like source in CO. The calibration for the beam efficiency is done by observing spectra of M17SW (R.A., Dec.) $_{J2000} = (18:20:23.1, -16:11:43)$ assuming that the peak radiation temperature (T_R^*) is 69.6 K (Wang et al. 1994). The data are reduced with NOSTAR, similar to the 45 m data, resulting in the final data cube with the effective spatial resolution of $24''.2$. The rms noise temperature (T_{rms}) of the spectra of each $7''.5$ grid cell are 0.13 K after calibration.

4. RESULTS

4.1. Spatial and velocity structures in $J=1-0$

Fig. 1 is the peak T_{MB} map of the CO $J=1-0$ line in the cloud boundary region of LDN 204. The west

side of the cloud is facing the H II region Sh 2-27 and the cloud surface is illuminated by UV flux from ζ Oph located in the direction of north west. The edge of the cloud does not appear to be a smooth surface, but has a complex morphology, for example, there is a prominent clumpy structure protruding to the west in the middle of the observed area. The velocity field is also remarkably complex as seen in the channel maps of Fig. 2.

Particularly a few prominent features can be recognized such as clumpy, pillar-like, and arc-like features as denoted by A, B, and C in Fig. 2, respectively. The clumpy structure is especially noticeable in the peak T_{MB} map as slightly detached from the main cloud. The clump (A) has a radius of $\sim 45''$, corresponding to $r \sim 6300$ AU. Using the empirical relation of $X \equiv N(\text{H}_2)/W(\text{CO}) = 1.56 \times 10^{20} \text{ cm}^{-2} (\text{K km s}^{-1})^{-1}$ (Hunter et al. 1997), the total mass of the clump is estimated to be $0.05 M_{\odot}$, where $N(\text{H}_2)$ is the column density of molecular hydrogen and $W(\text{CO})$ is the integrated intensity of the CO $J = 1-0$ line. Similar morphological structures have been discovered at interaction regions of the cloud surfaces with H II regions like M16 (e.g., Hester et al. 1996). They are referred to as ‘‘Evaporated Gaseous Globules’’ (EGGs). The size of the clump is, however, much larger than those of EGGs that range from 150 AU to 1800 AU. The pillar-like feature (B) is visible in the channels around $V_{\text{LSR}} \approx 5.4 \text{ km s}^{-1}$ and overlapping with other velocity components. It is roughly pointing to the direction of the UV radiation source of ζ Oph. The arc-like feature (C) is protruded from the main cloud by ~ 7000 AU, and if it is assumed to be a bent cylinder, its radius is $r \sim 3000$ AU.

4.2. Velocity dispersions of the small scale structures

The CO $J = 1-0$ line profiles at the peaks of the 3 prominent features and a typical line profile in the middle of the cloud are investigated. Fig.3 illustrates that the lines at the 3 positions are fitted to single or double gaussian profiles and the central velocities and velocity dispersions are estimated. For positions A and C, the line emissions are fitted to single gaussians whose Full Width Half Maximum (FWHM) line widths are 0.57 km s^{-1} and 0.51 km s^{-1} , respectively. At position B, the line has clear double components, which have FWHM of 0.63 km s^{-1} and 0.59 km s^{-1} . The central velocities are clearly different ranging from 3.8 km s^{-1} to 5.3 km s^{-1} . On the other hand, in the middle of the cloud, the spectral line shapes are not well fitted to the gaussian profile, but more irregular. They seem to be saturated at typical peak antenna temperature of ~ 6 K, and consist of multiple velocity components overlapping on the line of sight forming large velocity dispersion. The composite average spectrum over the entire observed area is illustrated by the black line in Fig. 3. The gaussian fitting to it gives a much larger line width of $\sim 1.5 \text{ km s}^{-1}$ than those of the small-scale structures (hereafter 0.6 km s^{-1} component).

The observed line width is composed of thermal and non-thermal components expressed as $\Delta V_{\text{obs}}^2 = \Delta V_{\text{th}}^2 + \Delta V_{\text{NT}}^2$, where the thermal component of the velocity dispersion at temperature T is expressed as $\Delta V_{\text{th}} = \sqrt{8 \ln 2 \cdot kT/m}$ where k is the Boltzman’s constant and m is the mass of the molecule. For the cases of $T =$

20, 60, 150 K, ΔV_{th} of the ^{12}CO molecule is calculated to be 0.2, 0.35, 0.55 km s^{-1} , respectively. Because we do not expect temperatures as high as 1000 K for molecular clouds, typical line widths of $\sim 1.5 \text{ km s}^{-1}$ have been interpreted as turbulent rather than thermal motion. The velocity dispersion of $\sim 0.6 \text{ km s}^{-1}$ implies, on the contrary, that the cloud small structures are nearly thermalized with temperature of ~ 150 K, or they have relatively small non-thermal components.

These results imply that the molecular cloud is not made of a uniform material, but composed of small-scale cloudlets whose internal velocity dispersion is as small as the thermal motion of CNM, while the relative motion of the individual cloudlets is much larger. Because many small-scale cloudlets are overlapping on the same line of sight in the main cloud, the spectral lines obtained in the middle of the cloud are widened and exhibit larger line width mimicking supersonic motion of the entire material in the cloud. The relative motion of the cloudlets is in fact in the order of $1-2 \text{ km s}^{-1}$, which is supersonic with respect to the temperature of CNM ($T \sim 50$ K), but subsonic with respect to WNM ($T \sim 8000$ K). This interpretation is consistent with the two-phase medium turbulent model of Koyama & Inutsuka (2002).

4.3. CO $J = 3-2$ results

The data of ASTE CO $J = 3-2$ and 45 m $J = 1-0$ are compared in detail for the purpose of investigating the gas density and temperature of the small-scale cloud structures. In order to make a point-to-point comparison, the 45 m data are spatially convolved with a gaussian beam of $22''$ HPBW so that the 2 datasets have the same spatial resolution.

Fig. 4 illustrates the peak T_{MB} ratio of $R_{3-2/1-0}$ for the 2 regions where (a) the clumpy and (b) the arc-like features are detected. In region a, the clumpy feature entirely has $R_{3-2/1-0} \geq 1$ and at the peak position a1, $R_{3-2/1-0} \approx 1.4$. The west side of the clump facing the H II region has even higher ratio of $R_{3-2/1-0} \approx 2$ at position a2. The west side of the clump has a steep intensity gradient and is illuminated by strong UV radiation, so the gas temperature is expected to be higher than the eastern side. Both of the $J = 1-0$ and $3-2$ lines at positions a1 and a2 have line widths of $\sim 0.6 \text{ km s}^{-1}$, while in the periphery at a3 and a4, their line widths are significantly larger than $\sim 1.5 \text{ km s}^{-1}$ (Fig. 5a). In region b, the arc-like feature shows a similar trend of $R_{3-2/1-0}$ having higher values in the west side. At the peak position b1, $R_{3-2/1-0}$ is close to unity. The $J = 3-2$ lines’ intensity and shapes resemble the $J = 1-0$ lines in general as seen at positions b1, b2, and b3.

5. DISCUSSION

5.1. Physical properties of the small scale molecular cloud

In the observed region, there are small scale structures detected near the main cloud boundary, i.e., the 0.6 km s^{-1} width component whose typical size is $6000 \text{ AU} \lesssim l \lesssim 12600 \text{ AU}$. According to the theory of Koyama & Inutsuka (2002), thermal instability of shock-compressed WNM ($T \sim 8000$ K) forms thermalized cloudlets of a few 100 AU made of CNM ($T \sim 50$ K) that are embedded in the WNM. They have random motion with a velocity

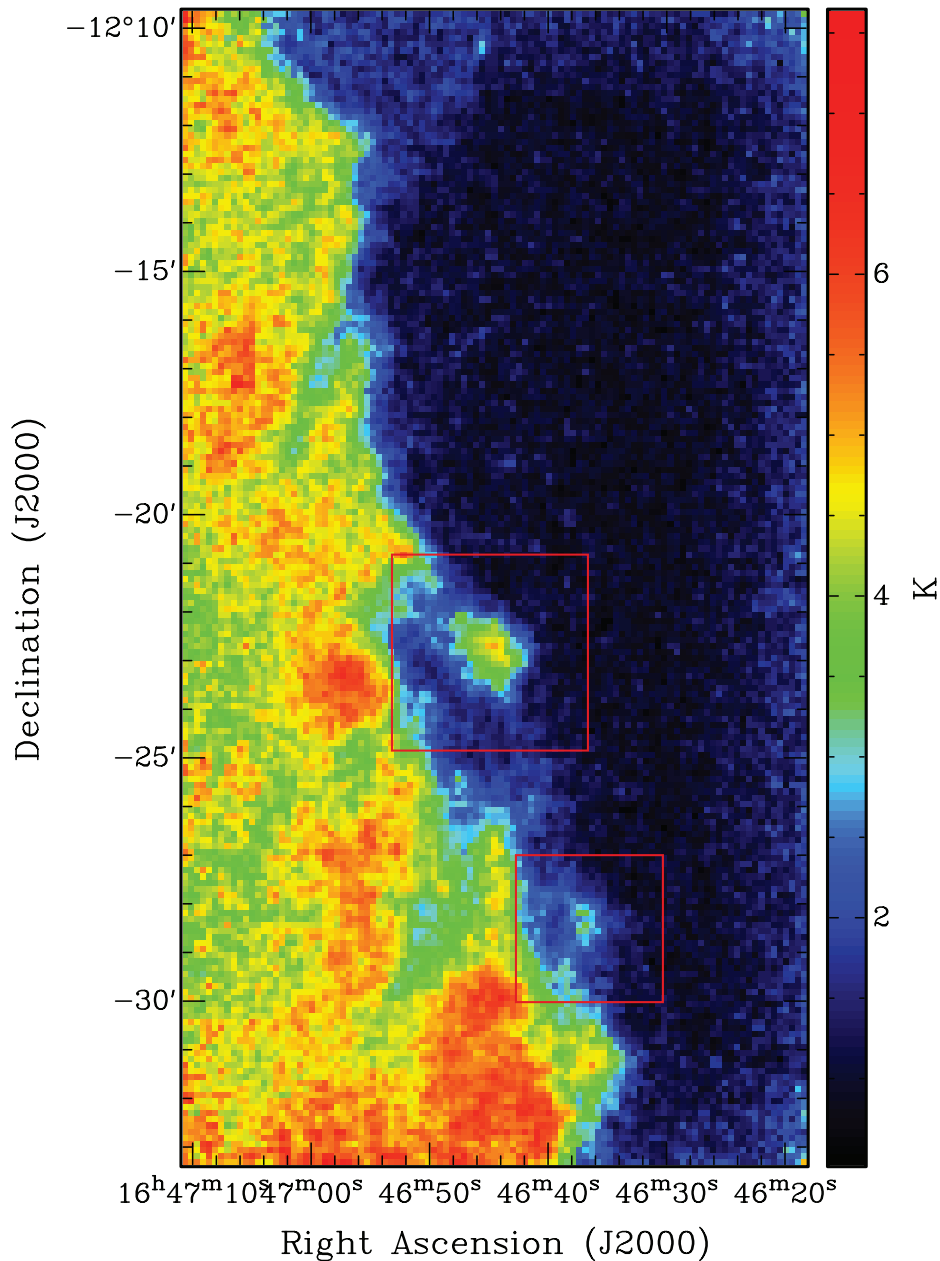


Figure 1. Pseudo color image of peak T_{MB} map in CO $J = 1-0$ observed with the NRO 45 m telescope. The two red squares denote the regions where CO $J = 3-2$ data are taken with ASTE.

dispersion of a few km s^{-1} and coalesce with each other to form larger structures up to several $\times 1000$ AU. Our results are consistent with this scenario from the morphological and kinematical point of view. In order to further corroborate the theory, estimation of gas density and temperature are attempted in the following.

The 0.6 km s^{-1} width component is well traced by both of the CO $J = 1-0$ and $3-2$ lines. The gas density and temperature can be constrained from the intensities of multiple lines by the large velocity gradient (LVG) analysis, which requires density, temperature, column density, abundance, and velocity gradient. For the calculation, we adopt flowing assumptions setting the density ($n(\text{H}_2)$) and the kinetic temperature (T_{kin}) as free parameters. 1) H_2 density ($n(\text{H}_2)$), CO abundance ratio to H_2 (Z), and column density ($N(\text{CO})$) have the rela-

tion of $N(\text{CO}) = Zn(\text{H}_2)l$ where l is the path length of the cloud along the line of sight. 2) The path lengths (l) are the same as the apparent diameters of the clouds ($2 \times r$), i.e., spherical or axial symmetry. 3) The velocity gradients are the same as the CO $J = 1-0$ line widths divided by the path lengths ($\Delta V/l$). 4) The CO abundance is constant as $Z \sim 3 \times 10^{-5}$ for the entire clouds. The last assumption is, however, unlikely because the present region is under strong UV radiation and a considerable amount of CO molecules is dissociated to be C I, particularly at the cloud surface. We therefore tested the calculation altering the CO abundance with 3 different Z values of 5×10^{-5} , 1×10^{-5} , and 5×10^{-6} . As a result, it is found that the response of $R_{3-2/1-0}$ to the same $n(\text{H}_2)$ and T_{kin} changes with Z by a factor of 3 or less, while the velocity integrated CO intensity, $W(\text{CO})$,

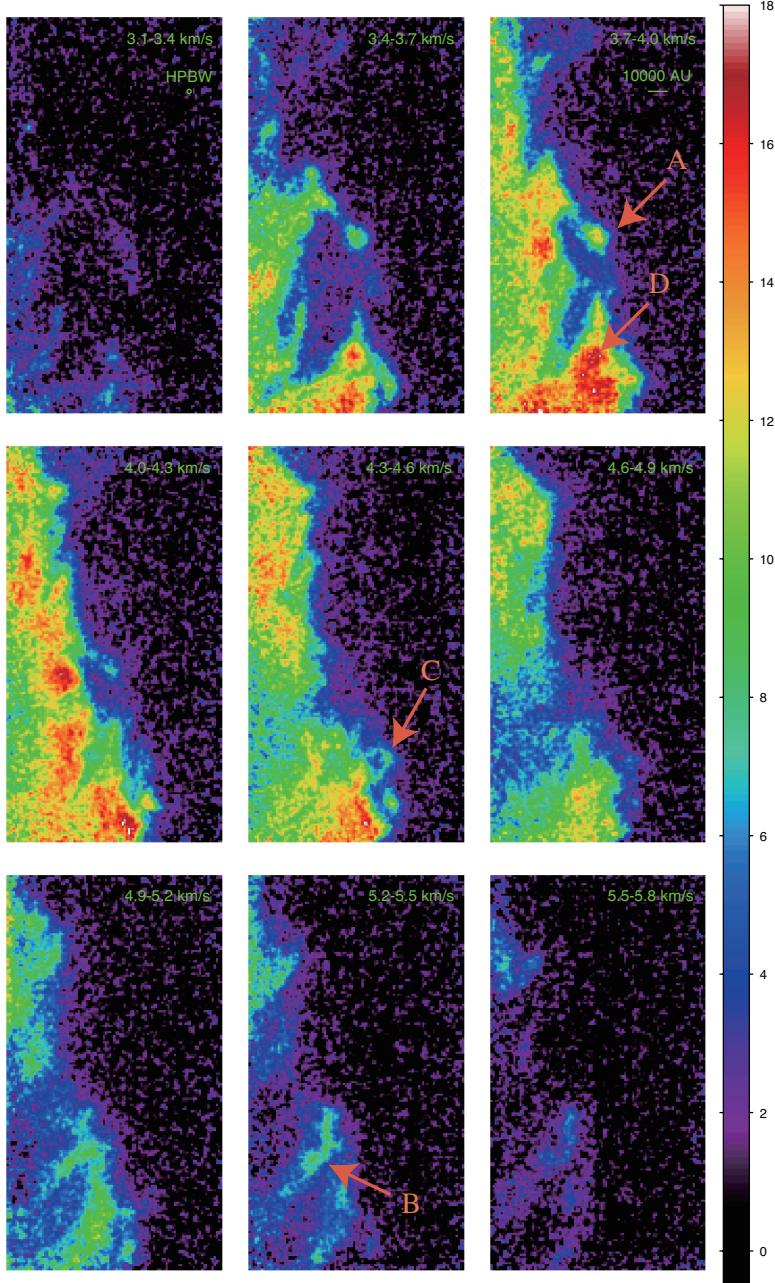


Figure 2. Channel map of the CO $J = 1-0$ emission for the same region as Fig. 1. Each map shows CO intensity integrated over 0.3 km s^{-1} velocity width as shown at the top right of each map. Three prominent structures (the clump, pillar and arc) are designated by A, B, and C, respectively, in addition to a middle part of the cloud by D. The data used to create this figure are available in the online journal.

changes up to an order of magnitude.

Figs. 6 illustrate the results of the LVG calculations showing $R_{3-2/1-0}$ as a function of $n(\text{H}_2)$ and T_{kin} by gray scale and contours. Fig. 6a is for the case of $\Delta V = 0.6 \text{ km s}^{-1}$ and $l = 12600 \text{ AU}$, corresponding to the clumpy structure, which demonstrates the line ratio is in the range of $1 < R_{3-2/1-0} < 2$ for the entire region, while the integrated intensity $W(\text{CO})$ in the clumpy structure is between 2.5 and 4.0 K km s^{-1} for the $J = 1-0$ line. The parameter set of $n(\text{H}_2)$ and T_{kin} that meets these observed conditions does not exist in this figure with $T_{\text{kin}} < 300 \text{ K}$ for the case of $Z = 5 \times 10^{-5}$. For the lower abundance cases, these conditions are satisfied with the parameter in the shaded areas of Fig. 6a. For the

case of $Z = 1 \times 10^{-5}$, the density and kinetic temperatures are restricted to be $1000 \lesssim n(\text{H}_2) \lesssim 3000 \text{ cm}^{-3}$ and $100 \lesssim T_{\text{kin}} \lesssim 300 \text{ K}$; and for $Z = 5 \times 10^{-6}$, they are $2500 \lesssim n(\text{H}_2) \lesssim 6000 \text{ cm}^{-3}$ and $40 \lesssim T_{\text{kin}} \lesssim 120 \text{ K}$. These are warmer and denser compared to typical dark clouds detected in ^{12}CO . From the size and thus constrained density, the mass of the clump is given as $0.008 \lesssim M \lesssim 0.05 M_{\odot}$, which is below the brown-dwarf mass limit. Since these masses are well below the Jeans mass at their current densities, these cloudlets are not expected to collapse gravitationally. Their further evolution may include mutual coalescence, condensation from surrounding medium, “evaporation” (from cold gas to warm gas), and photo-dissociation.

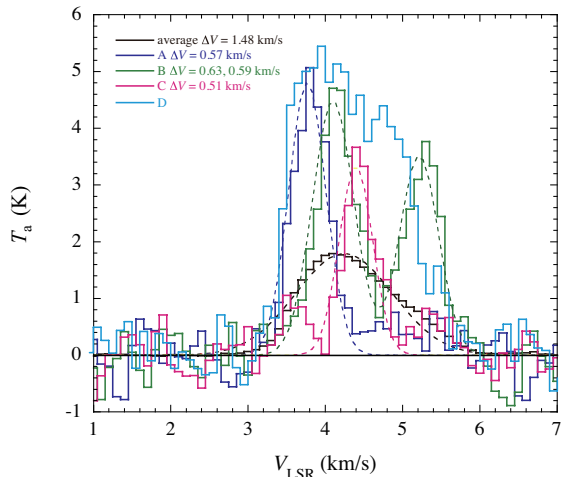


Figure 3. Spectra of the CO $J = 1-0$ line at the 3 peak positions of the clumpy (A in blue), pillar-like (B in green), arc-like (C in magenta) structures, and the middle of the cloud (D in cyan) as shown in Fig. 2. The black curve illustrates the average CO $J = 1-0$ spectrum of the entire observed region. The dotted curves are the gaussian profiles fitted to those spectra, whose line width (FWHM) are indicated in the top-left of the figure.

Fig. 6b is for $l = 6000$ AU and $\Delta V = 0.6 \text{ km s}^{-1}$ as for the arc-like structure, illustrating the similar trend, but using the same $n(\text{H}_2)$ and T_{kin} , $R_{3-2/1-0}$ is calculated to be higher and $W(\text{CO})$ is lower than Fig. 6a, yielding lower kinetic temperature for the same $R_{3-2/1-0}$ value and require higher density for the same $W(\text{CO})$. Note that in the area on the left side of the turn-over point of the $R_{3-2/1-0}$ contours, both lines are optically thin. As seen in Fig. 4b, the arc-like structure exhibits higher $R_{3-2/1-0}$ than unity for the entire structure, and the peak ratio is ~ 2 around the position b4. The integrated intensity of the $J = 1-0$ line in this structure is in the range between 2.0 and 3.5 K km s $^{-1}$. Hence, as for Fig. 6a, there is no region meeting the observed constraints with $T_{\text{kin}} < 300$ K and $Z = 5 \times 10^{-5}$, while we obtained a satisfying region for the lower abundance cases. For the case of $Z = 1 \times 10^{-5}$, the density and kinetic temperatures are constrained as $2000 \lesssim n(\text{H}_2) \lesssim 5000 \text{ cm}^{-3}$ and $50 \lesssim T_{\text{kin}} \lesssim 150$ K; and for the case of $Z = 5 \times 10^{-6}$, $4000 \lesssim n(\text{H}_2) \lesssim 11000 \text{ cm}^{-3}$ and $25 \lesssim T_{\text{kin}} \lesssim 60$ K. These imply that the arc-like structure is cooler and denser than the clumpy one. From the derived density range, the mass of the arc-like structure is also constrained to be very low-mass as $0.005 \lesssim M \lesssim 0.03 M_{\odot}$.

If we use the empirical relation of $N(\text{H}_2) = X \cdot W(\text{CO})$ with an assumption of $X = 1.56 \times 10^{20} \text{ cm}^{-2} (\text{K km s}^{-1})^{-1}$ (Hunter et al. 1997), the average density is thus derived only from $W(\text{CO})$ and l as $\sim 3300 \text{ cm}^{-3}$ and $\sim 6000 \text{ cm}^{-3}$ for the clumpy and arc-like structures, respectively. Under the circumstance with strong UV radiation, smaller Z and thus larger X are expected than above, yielding larger density, and therefore consistent density estimations are plausible. Nevertheless, these estimates are uncertain under such an extreme condition.

Although the mean kinetic temperature of molecular gas along the line of sight toward ζ Oph was estimated to be 54 K from H_2 absorption (Savage et al. 1977; Liszt et al. 2009), small scale structures may have large temperature variations. The estimated kinetic temperature

of the 0.6 km s^{-1} component is relatively high compared to typical dark clouds, but they are still much colder than WNM. Tachihara et al. (2000b) reported that the entire LDN 204 cloud complex is a 20-pc long and 2-pc wide filament with an estimated mass of $1100 M_{\odot}$, yielding the average density of $\sim 250 \text{ cm}^{-3}$. The above calculations reveal the clumpy and arc-like structures to be 4 to 40 times denser than the cloud average.

5.2. Other observational evidence of small-scale cloud structures

From observational points of view, some studied have been published attempting to investigate small-scale structures of ISM. Sakamoto (2002) and Sakamoto & Sunada (2003) detected similar small-scale structures at the edge of high-latitude clouds (MBM 54 and MBM 55) and Heiles Cloud 2 in Taurus, respectively, although their observations were by one-dimensional strip scan. The typical one-dimensional size is ~ 10000 AU, comparable to our 0.6 km s^{-1} structures, while their FWHM line widths are $\simeq 1.8$ and $\simeq 2.8 \text{ km s}^{-1}$ for MBM 54 and MBM 55, and $\simeq 2 \text{ km s}^{-1}$ for HCL2, respectively, significantly larger than the present results. Without strong UV radiation, these regions are supposed to have smaller pressure and remarkably low density of $n(\text{H}_2) \leq 100 \text{ cm}^{-3}$ is estimated, although no detailed estimation of the physical cloud parameter was performed. These clouds with different velocity widths may have been caused by different initial conditions.

Falgarone et al. (2009) investigated even smaller-scale structures using the IRAM-PdB interferometer in the Polaris Flare, and detected elongated structures of ~ 300 AU thickness. They tend to be seen in the CO $J = 1-0$ line wings with line width of $0.1-0.4 \text{ km s}^{-1}$. Because some of the elongated structures form parallel pairs with different velocity, it was suggested that the small structures are thin layers of CO cloud with velocity shears driven by turbulent flow.

At high galactic latitude, small-scale CO structures have been discovered by single-dish survey and by interferometry. Heithausen (2002) serendipitously discovered small-scale ($< 1'$) structures with $\Delta V \sim 0.8 \text{ km s}^{-1}$ with the IRAM 30m telescope. The clouds are resolved into smaller-scale (\sim a few $10''$) structures with $\Delta V \sim 0.4 \text{ km s}^{-1}$ by the PdBI interferometric observation (Heithausen 2006). Assuming the distance of 100 pc, their sizes and densities are \leq a few $\times 100$ AU and $\geq 20,000 \text{ cm}^{-3}$, respectively. By a follow-up large-scale survey, Heithausen (2006) claimed that such small clouds are common in the ISM, but their total mass amounts to only $< 1\%$ of the whole gas mass. The size and ΔV of the small-scale structures ranging from ~ 100 AU to 10^4 AU including an ensemble cloud have a correlation of $\Delta V \propto r^{0.3}$, where r is the effective radius of the cloud. Our sample of the 0.3 km s^{-1} and the 0.6 km s^{-1} width components roughly fit to the correlation.

Ingalls et al. (2007) observed MBM-12 with OVRO interferometer and detected 1-5 milli-parsec scale clouds in the CO line wings. They discussed that the velocity field of the cloud is made of an ensemble of tiny diluted turbulent cells.

In the course of the natal cloud survey of the young stellar cluster TW Hya association, Tachihara et al.

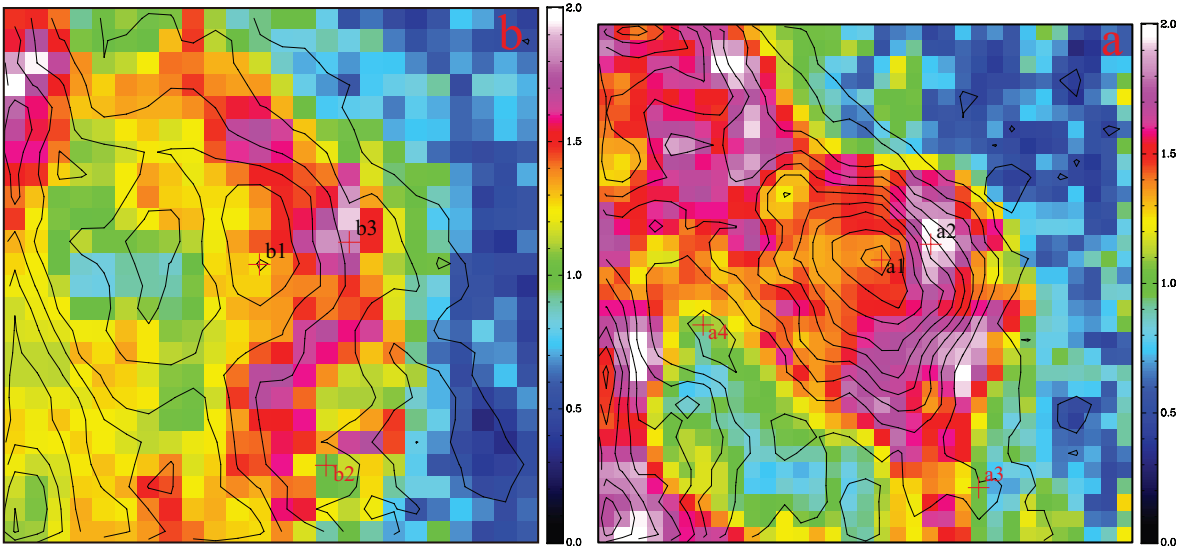


Figure 4. Pseudo color image of the peak T_{MB} ratio of $R_{3-2/1-0}$ around the clump (a), the arc (b), respectively. Overlaid are contours of peak T_a $J=1-0$ from 1.0 K ($=2.7\sigma$) with 0.4 K steps. The coordinates of the center positions are (16:46:45.0, -12:22:50) and (16:46:36.5, -12:28:30), respectively, and the sizes of the maps are $4' \times 4'$ and $3' \times 3'$, respectively, as denoted by the red boxes in Fig. 1.

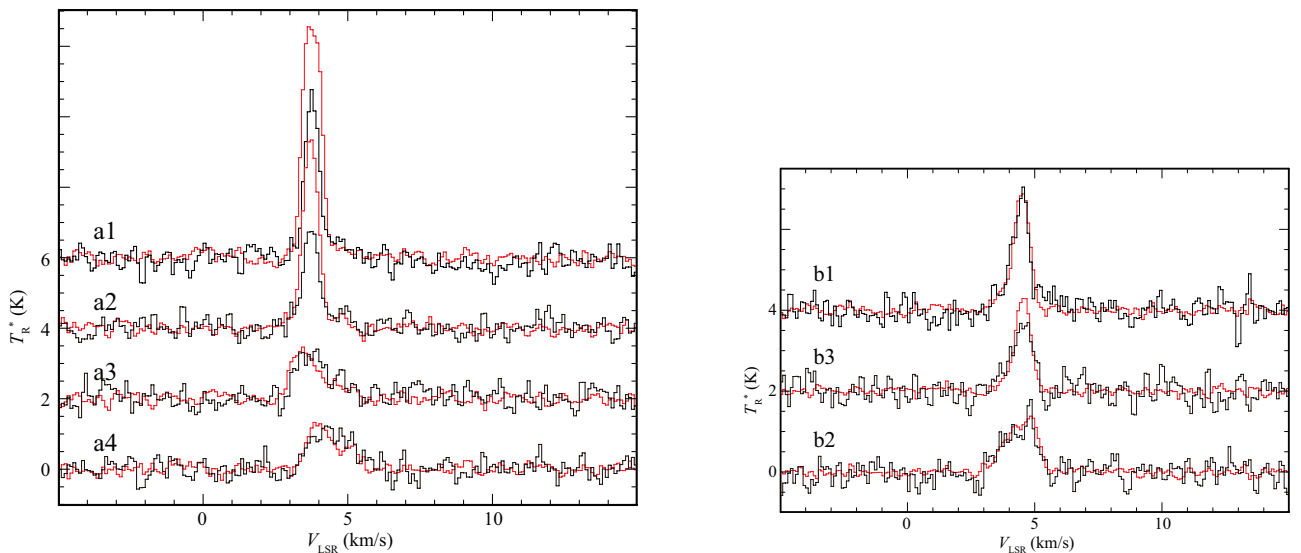


Figure 5. Spectra of CO $J=1-0$ (black) and $3-2$ (red) at the positions marked in Fig. 4. The CO $J=1-0$ data are convolved with a gaussian beam of $22''$ HPBW so that the 2 data cubes have the same spatial resolution. The intensity and the spectral shapes of the emission lines of $\Delta V \sim 0.6$ km s^{-1} are similar for both transitions except for a1 and a2. The data used to create Figures 4 and 5 are available in the online journal.

(2009) detected small clouds by the NANTEN telescope. They have complex velocity structures and patchy morphology, barely resolved by the low spatial resolution observation ($2.7''$), but the line width is relatively narrow as ~ 1 km s^{-1} . Some of them are, on the other hand, revealed to have small distance (< 100 pc), indicated by the optical Na absorption lines. This ensures that the total molecular mass derived from CO within the surveyed area of 1.9 deg 2 is $\lesssim 3 M_\odot$. These results suggest that such small-scale cloud structures are common in the ISM.

5.3. Nature of the small-scale structures and origin of interstellar turbulence

As for the physical nature of the ubiquitous interstellar turbulence from diffuse to dense gas, the Kolmogorov model has been supposed to be a plausible mechanism. According to the model, turbulence is driven by a larger-scale wave such as a supernova explosion, stellar wind, and molecular outflows, and cascades into smaller-scale structures. This cascade results in an energy spectrum expressed by a power-law function as $E(k) \propto k^{-5/3}$ where E is the energy of the turbulent flows and k is the wave number. Some observational results support this model (e.g., Armstrong et al. 1995), however, the driving mechanism is known to have a difficulty that the large-scale supersonic flows cause shock dissipation and most of the input energy is rapidly lost by

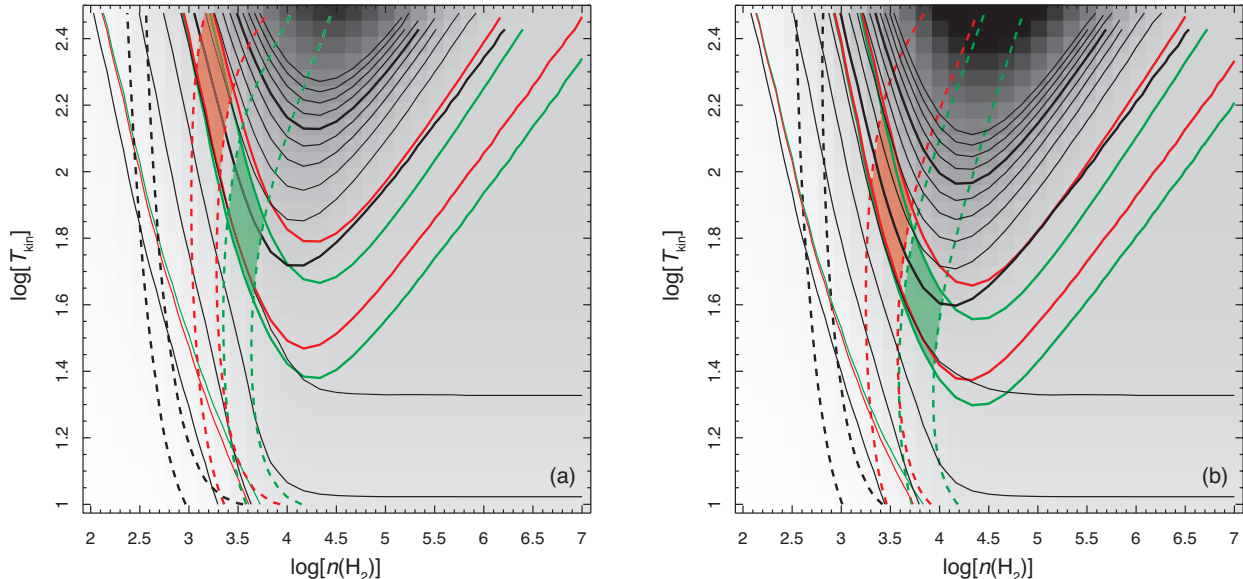


Figure 6. Intensity ratio diagrams of CO $R_{3-2/1-0}$ as a function of molecular hydrogen density ($n(\text{H}_2)$) and kinetic temperature (T_{kin}) shown by the gray scale and contours assuming the CO abundance of 5×10^{-5} . Contours are from 0.2 to 2.8 with steps of 0.2, and the bold contours indicate the line ratio of unity and 2. The red and green lines are contours of 0.2, 1.0 and 2.0 for the cases of lower CO abundance with $Z = 1 \times 10^{-5}$ and 5×10^{-6} , respectively. Used parameters are (a) $l = 12600$ AU and $\Delta V = 0.6$ km s $^{-1}$ and (b) $l = 6000$ AU and $\Delta V = 0.6$ km s $^{-1}$. The calculated integrated intensity of CO $J=1-0$ under the given condition are shown by dotted contours of 2.5 and 4.0 K km s $^{-1}$ for (a) and 2.0 and 3.5 K km s $^{-1}$ for (b), respectively. The shaded areas indicate the parameter ranges meeting the observed values (see text).

radiation. In order to solve this problem, many magneto-hydrodynamic (MHD) simulations have been attempted with a help of the magnetic Alfvén wave. Nevertheless, it is reported that the MHD turbulence decays within a timescale of the order of the flow crossing time even with strong magnetic fields (Mac Low et al. 1998; Stone et al. 1998), because the cascade of the MHD turbulence happens within an eddy turnover time (Cho & Lazarian 2005).

According to the two-phase medium model, on the other hand, the molecular clouds in turbulent interstellar medium are built up from small scale structures formed by thermal instability and their coalescence. The ISM consist of two-phase gas, WNM and CNW, that can weaken the shock dissipation of the supersonic motion and prolong the decay time of turbulence (Inutsuka et al. 2005). In the ρ Ophiuchi cloud, CO and C I gas is reported to be well mixed (Kamegai et al. 2003), which supports the idea of the two-phase medium. If a cloud is interacting with an H II region like the present case, the cloud surface is exposed to the ionization shock, that produces turbulence via the thermal instability. The detection of the small scale structures with cold temperatures and high densities is strong support for the two-phase medium model.

In addition to the results of density distribution of the original work by Koyama & Inutsuka (2002), Yamada et al. (2007) further investigated the two-phase model including the radiative transfer calculation to estimate the temperature distribution as well as calculation of the line ratios of CO and C II emissions. They suggested that the small-scale CNM are formed from WNM via thermal instability having a small dense structure with minimum temperature of ~ 50 K, and the estimated $R_{3-2/1-0}$ is

between 2 and 3, slightly higher than our result. Their condition is, however, set to be lower density ($n(\text{H}_2) \lesssim 3000$ cm $^{-3}$), and for the case of higher density and lower temperature, $R_{3-2/1-0}$ is expected to be smaller.

Note that the numerical simulations of Koyama & Inutsuka (2002) and Yamada et al. (2007) begin with uniform WNM compressed by passage of a shock wave. Koyama & Inutsuka (2002) showed that if the pre-shock gas is essentially one-phase diffuse WNM, the thermal instability induced by shock compression results in forming two-phase turbulent medium. However, the present case of our observed molecular cloud (CNM) is supposed to be clumpy (multi-phase) medium that preexists even before the UV ionization takes place. This is because the UV source of ζ Oph is a run-away star, it has been irradiating the cloud only for a few $\times 10^5$ yrs, which is shorter than the timescale of thermal instability (Tachihara et al. 2000b). In addition, the molecular CO gas seems to be well mixed with atomic C I gas even in dense parts of the cloud (Kamegai et al. 2003), the ISM in this region is supposed to be clumpy two-phase medium even before the interaction with ζ Oph. On the other hand, using MHD simulations, Inoue et al. (2009b, 2011) revealed, however, that passage of shock wave through the two-phase medium drives the ISM turbulence owing to vortex creation by shock-cloud interaction. This mechanism does not require thermal instability, and hence, the turbulence is driven more effectively with shorter timescale than the gas cooling time, and even shorter than the crossing time of ζ Oph. It is also anticipated that under the strong UV radiation the ISM should have larger turbulence due to larger input energy causing larger line width (Tachihara et al. 2000a, 2002; Gritschneider et al. 2009).

In order to further study the origin of interstellar turbulence, high resolution interferometric observations in multi-transition CO lines at cloud boundaries are required. Also for the investigation of physical properties of WNM, extensive C I observation in the submm wavelength is highly desired. Observational results brought by ALMA combined with ACA would enormously improve our understanding in the near future.

6. SUMMARY

In order to investigate the origin of interstellar turbulence and verify the theoretically proposed thermal instability model of two-phase medium, we have carried out CO $J=1-0$ and $3-2$ observations toward a boundary between LDN 204 dark cloud and an H II region Sh 2-27. The main conclusions are as follows.

1. By detailed investigation of spatial and velocity distribution of CO $J=1-0$, small-scale cloud structures have been discovered.
2. They have characteristic morphologies such as clumpy, arc-like, and pillar-like structures, which appear in some velocity channels with typical size scale of a few $\times 1000$ AU to 12000 AU and the velocity dispersion of $\Delta V \sim 0.6$ km s $^{-1}$. The systemic velocities of these 0.6 km s $^{-1}$ width component clouds have scatter of a few km s $^{-1}$.
3. The spectral line profile taken in the middle of the main cloud, and the composite line profile of the entire cloud resemble single component broad-line spectra with velocity dispersion several times larger than the typical sound speed. These facts suggest that the cloud is composed of tiny cloudlets with small internal velocity dispersion. Because of their relative motion and overlapping effect on the line of sight, molecular clouds are observed to have supersonic turbulence as a whole.
4. Follow-up observations in CO $J=3-2$ for these small structures revealed that the intensity ratio of $R_{3-2/1-0}$ is close to unity for the 0.6 km s $^{-1}$ width component, which shows minimum kinetic temperature of $T_{\text{kin}} > 25 - 100$ K, relatively higher than typical dark clouds.

5. From the LVG analysis, it is found that the 0.6 km s $^{-1}$ width components have average density of $\sim 10^{3-4}$ cm $^{-3}$, much higher than the entire cloud average density. Owing to their small sizes, masses of the 0.6 km s $^{-1}$ width components are estimated to be $0.005 \lesssim M \lesssim 0.05 M_{\odot}$, well in the domain of brown-dwarf mass.
6. These results strongly support the theoretical thermal instability model of two-phase medium first proposed by Koyama & Inutsuka (2000, 2002). We conclude that the interstellar turbulence is likely to be driven by thermal instability and the small-scale structures are the building blocks of the turbulent molecular clouds.

We are grateful to staff members of the Nobeyama radio observatory and the ASTE support team. We thank Miyuki Murai for helping with the 45 m telescope observations and Takeshi Tsukagoshi for the ASTE observations. Nobeyama Radio Observatory is a branch of the National Astronomical Observatory of Japan, National Institutes of Natural Sciences. The ASTE project is driven by Nobeyama Radio Observatory (NRO), a branch of National Astronomical Observatory of Japan (NAOJ), in collaboration with University of Chile, and Japanese institutes including University of Tokyo, Nagoya University, Osaka Prefecture University, Ibaraki University, and Hokkaido University. Observations with ASTE were in part carried out remotely from Japan by using NTT's GEMnet2 and its partner R&E (Research and Education) networks, which are based on AccessNova collaboration of University of Chile, NTT Laboratories, and NAOJ. This work is financially supported by the Grants-in-Aid for the Scientific Research by the Ministry of Education, Science, Sports and Culture (No. 23540277 and 23740154). This publication is supported as a project of the Nordrhein-Westfälische Akademie der Wissenschaften und der Künste in the framework of the academy program by the Federal Republic of Germany and the state Nordrhein-Westfalen.

APPENDIX

INTERSTELLAR DUST COMPONENT OF THE CLOUD

Besides the molecular and ionized gas components, dust is an important content of the ISM. The emission, absorption and scattered light by the interstellar dust can provide morphological, geometrical and temperature information of the cloud.

An H α image was obtained toward the entire cloud complex of LDN 204 with VYSOS-6 A, a 150 mm telescopes of the Universitätssternwarte Bochum in Chile. Ten images each with an integration time of 2 minutes were taken during March 24th and 25th 2012. The images were taken with an H α filter whose central wavelength and the FWHM are 656 nm and 5 nm, respectively, and in dither-mode for bad-pixels removal. After dark and bias subtraction and flatfielding the images were combined using a min/max-rejection. The reduced image was then binned (8×8) and low-pass filtered. In the observed region, the extinction of H α is not as prominent as in the main filament of LDN 204, but visible as a dark nebular near the edge of the spherical H II region Sh 2-27 (Fig. 7). This ensures that the entire cloud is located in front of the Strömgren sphere and gas is accelerated toward us by the UV light (Tachihara et al. 2000b).

The global distribution of the CO emission is compared with the dust thermal emission in 100 μm by Tachihara et al. (2000b). They are in good agreement in general, but the 100 μm emission is enhanced at the cloud surface irradiated by the UV light. The dust temperature distribution is represented by the color of far-IR thermal emission.

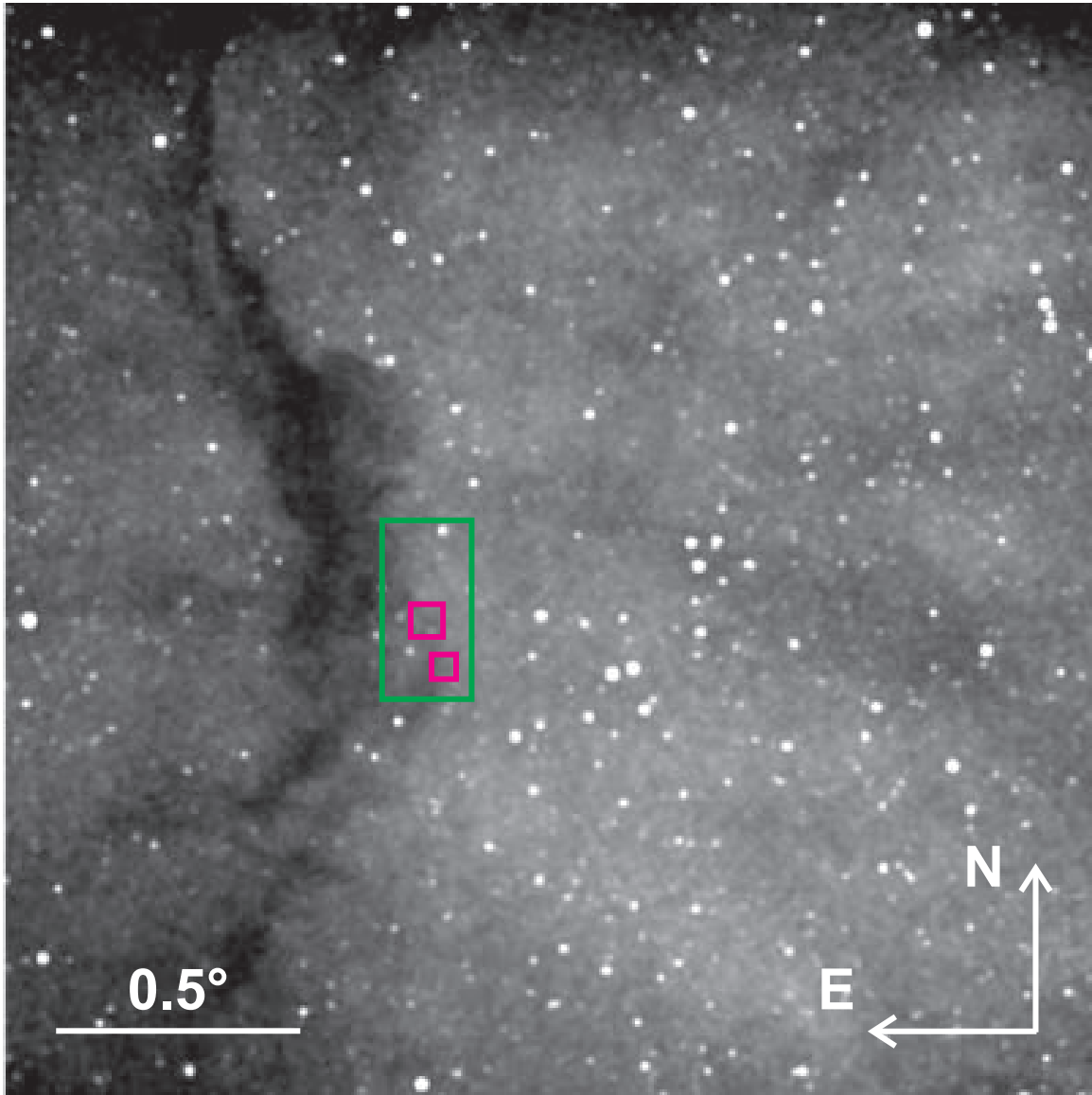


Figure 7. $H\alpha$ image ($2^{\circ}25 \times 2^{\circ}25$) of the LDN 204 cloud around the target region taken by the VYSOS-6 A telescopes at the Universitätssternwarte Bochum in Chile. The regions observed by the 45m telescope and ASTE are designated by green and magenta rectangles, respectively.

Fig. 8 is the 3-color composite image of the entire region of LDN 204 produced with the Improved Reprocessing of the IRAS Survey (IRIS) data⁷. The cloud surface is heated by UV radiation and the dust has relatively high temperature as demonstrated by the enhanced $60 \mu\text{m}$ emission over $100 \mu\text{m}$. The local high temperature causes the enhancement of $100 \mu\text{m}$ emissivity at the cloud surface relative to the CO line (Tachihara et al. 2000b). The dense parts of the cloud are, on the contrary, in low-temperature indicated by relatively strong emission in $100 \mu\text{m}$.

Recent preliminary release of the Wide-field Infrared Survey Explorer (WISE) data⁹ is compared with the CO distribution. Fig. 9 shows 3-color composite image in the region around LDN 204 using the band 4 ($22 \mu\text{m}$) in red, band 3 ($12 \mu\text{m}$) in green, and band 2 ($4.5 \mu\text{m}$) in blue. The $22 \mu\text{m}$ emission is supposed to come from small dust particles not in thermal equilibrium, while the $12 \mu\text{m}$ one is rather dominated by the emission from polycyclic aromatic hydrocarbons (PAH) excited by UV light (e.g., Compiègne et al. 2011). These mid-IR emission in general delineate the cloud surface facing the H II region, while the emission in $12 \mu\text{m}$ appears to be more spread than in $22 \mu\text{m}$. On the other hand, the dense part in the cloud traced by $\text{C}^{18}\text{O } J=1-0$ (Tachihara et al. 2000a) appears to be a dark lane in mid-IR, unlike at $100 \mu\text{m}$, slightly offset to the far side from ζ Oph. The dust in the cloud is supposed to have high column density and low temperature in the dark lane. The CO $J=1-0$ distribution of the present study traces the edge of the cloud where the column density is not so high but mid-IR is bright in emission. Besides the cloud's edge, diffuse mid-IR emission is extended outside the region detected in CO. It suggests that considerable amount of molecular gas is photo-evaporated by the UV radiation but the warm dust grains remain at the cloud surface. This

⁸ The IRIS data is obtained from <http://irsa.ipac.caltech.edu/data/IRIS/>

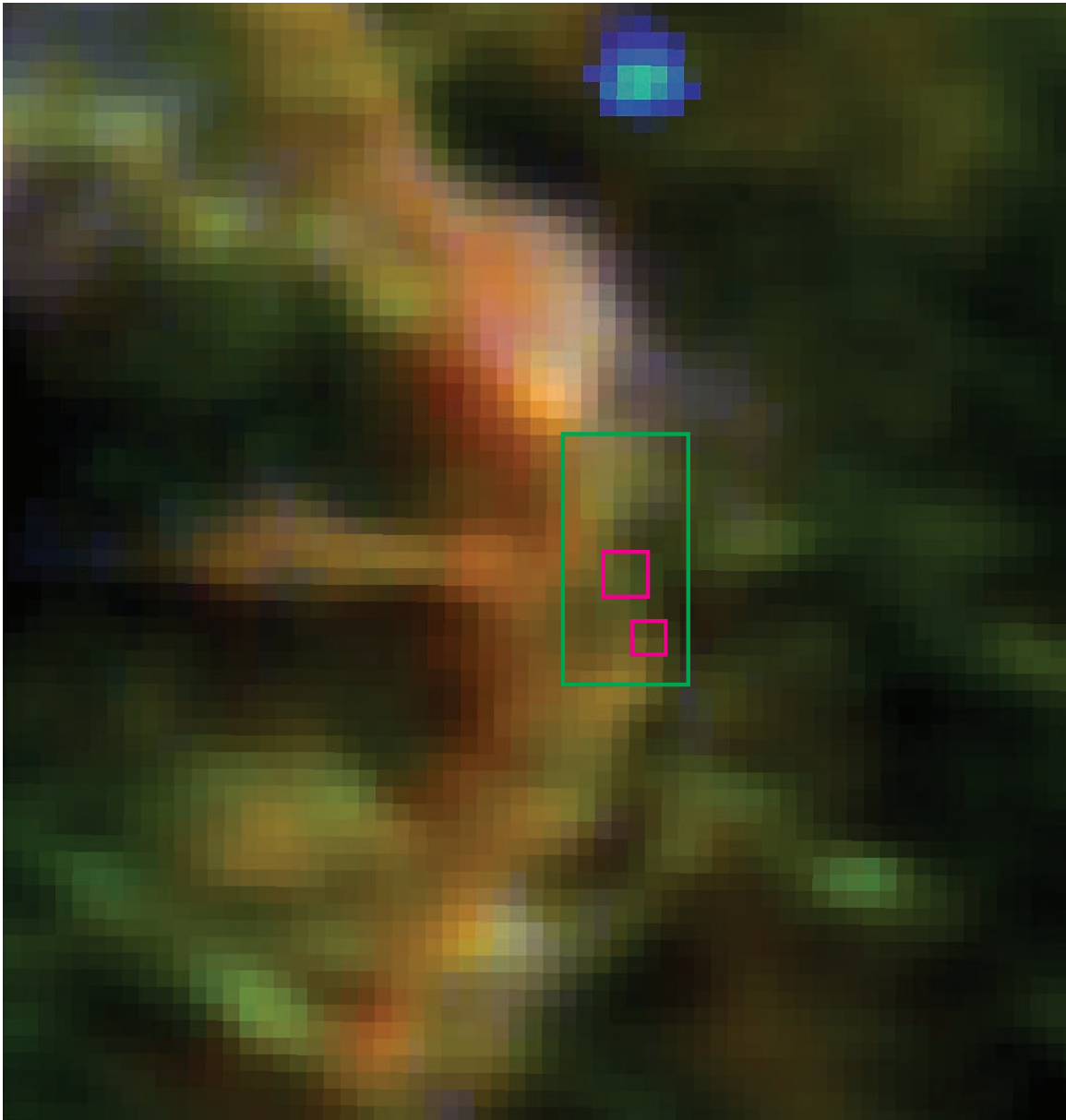


Figure 8. IRIS 3-color composite image of the LDN 204 cloud, $100' \times 100'$ around the target region ($12 \mu\text{m}$ in blue, $60 \mu\text{m}$ in green, and $100 \mu\text{m}$ in red). The regions observed by the 45m telescope and ASTE are designated by green and magenta rectangles, respectively.

feature is, on the contrary, not clearly visible in the absorption feature of $\text{H}\alpha$, implying that the warm dust cloud has relatively low column density.

REFERENCES

- Armstrong, J. W., Rickett, B. J., & Spangler, S. R. 1995, *ApJ*, 443, 209
 Cho, J., & Lazarian, A. 2005, *Theoretical and Computational Fluid Dynamics*, 19, 127
 Compiègne, M., Verstraete, L., Jones, A., et al. 2011, *A&A*, 525, A103
 Falgarone, E., Pety, J., & Hily-Blant, P. 2009, *A&A*, 507, 355
 Field, G. B., Goldsmith, D. W., & Habing, H. J. 1969, *ApJ*, 155, L149
 Gritschneider, M., Naab, T., Walch, S., Burkert, A., & Heitsch, F. 2009, *ApJ*, 694, L26
 Heithausen, A. 2002, *A&A*, 393, L41
 Heithausen, A. 2004, *ApJ*, 606, L13
 Heithausen, A. 2006, *A&A*, 450, 193
 Hennebelle, P., & Audit, E. 2007, *A&A*, 465, 431
 Hennebelle, P., Audit, E., & Miville-Deschênes, M.-A. 2007, *A&A*, 465, 445
 Hester, J. J., et al. 1996, *AJ*, 111, 2349
 Hunter, S. D., et al. 1997, *ApJ*, 481, 205

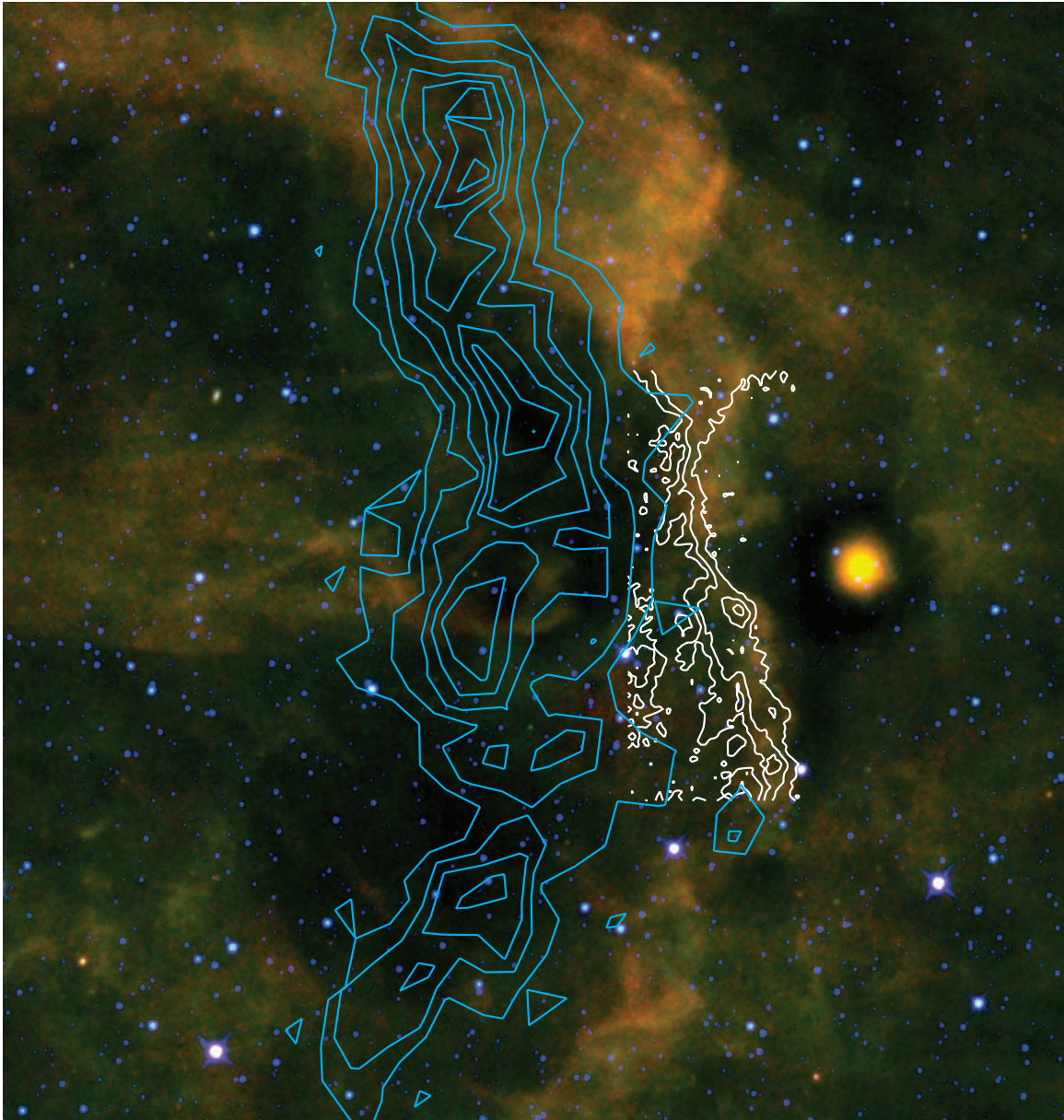


Figure 9. Composite 3-color composite image of WISE ($4.5 \mu\text{m}$ in blue, $12 \mu\text{m}$ in green, and $22 \mu\text{m}$ in red), 1 deg^2 around the LDN 204 cloud. The bright yellowish object in the right is a ghost of V446 Oph, which is out of the image. The white contours are the CO $J=1-0$ peak T_{MB} distribution by the present study with the 45m telescope, while those in cyan are the integrated intensity distribution of C^{18}O observed by Tachihara et al. (2000a) with the NANTEN telescope.

- Ingalls, J. G., Reach, W. T., Bania, T. M., & Carpenter, J. M. 2007, SINS - Small Ionized and Neutral Structures in the Diffuse Interstellar Medium, 365, 201
- Inoue, T., & Inutsuka, S. 2008, ApJ, 687, 303
- Inoue, T., & Inutsuka, S. 2009a, ApJ, 704, 161
- Inoue, T., Yamazaki, R., & Inutsuka, S. 2009b, ApJ, 695, 825
- Inoue, T., Yamazaki, R., Inutsuka, S., & Fukui, Y. 2011, ApJ, 744, 71
- Inutsuka, S., Koyama, H., & Inoue, T. 2005, Magnetic Fields in the Universe: From Laboratory and Stars to Primordial Structures., 784, 318
- Kamegai, K., et al. 2003, ApJ, 589, 378
- Koyama, H., & Inutsuka, S. 2000, ApJ, 532, 980
- Koyama, H., & Inutsuka, S. 2002, ApJ, 564, L97
- Lefloch, B., & Lazareff, B. 1994, A&A, 289, 559
- Liszt, H. S., Pety, J., & Tachihara, K. 2009, A&A, 499, 503
- Mac Low, M.-M., Klessen, R. S., Burkert, A., & Smith, M. D. 1998, Physical Review Letters, 80, 2754
- Mac Low, M.-M., & Klessen, R. S. 2004, Reviews of Modern Physics, 76, 125
- McCutcheon, W. H., Vrba, F. J., Dickman, R. L., & Clemens, D. P. 1986, ApJ, 309, 619
- Myers, P. C., & Goodman, A. A. 1991, ApJ, 373, 509
- Onishi, T., Mizuno, A., Kawamura, A., Ogawa, H., & Fukui, Y. 1996, ApJ, 465, 815
- Sakamoto, S. 2002, ApJ, 565, 1050

- Sakamoto, S., & Sunada, K. 2003, *ApJ*, 594, 340
Savage, B. D., Bohlin, R. C., Drake, J. F., & Budich, W. 1977, *ApJ*, 216, 291
Sawada, T., et al. 2008, *PASJ*, 60, 445
Shu, F. H., Adams, F. C., & Lizano, S. 1987, *ARA&A*, 25, 23
Stone, J. M., Ostriker, E. C., & Gammie, C. F. 1998, *ApJ*, 508, L99
Tachihara, K., Mizuno, A., & Fukui, Y. 2000a, *ApJ*, 28, 817
Tachihara, K., Abe, R., Onishi, T., Mizuno, A., & Fukui, Y. 2000b, *PASJ*, 52, 1147
Tachihara, K., Onishi, T., Mizuno, A., & Fukui, Y. 2002, *A&A*, 385, 909
Tachihara, K., Neuhäuser, R., & Fukui, Y. 2009, *PASJ*, 61, 585
Wang, Y., Jaffe, D. T., Graf, U. U., & Evans, N. J. 1994, *ApJS*, 95, 503
Yamada, M., Koyama, H., Omukai, K., & Inutsuka, S. 2007, *ApJ*, 657, 849